Nanoclusters

International Edition: DOI: 10.1002/anie.201908694
German Edition: DOI: 10.1002/ange.201908694

$Au_{130-x}Ag_x$ Nanoclusters with Non-Metallicity: A Drum of Silver-Rich Sites Enclosed in a Marks-Decahedral Cage of Gold-Rich Sites

*Tatsuya Higaki, Chong Liu, David J. Morris, Guiying He, Tian-Yi Luo, Matthew Y. Sfeir, Peng Zhang, Nathaniel L. Rosi, and Rongchao Jin**

Abstract: *The synthesis and structure of atomically precise $Au_{130-x}Ag_x$ (average $x = 98$) alloy nanoclusters protected by 55 ligands of 4-tert-butylbenzenethiolate are reported. This large alloy structure has a decahedral M_{54} ($M = Au/Ag$) core. The Au atoms are localized in the truncated Marks decahedron. In the core, a drum of Ag-rich sites is found, which is enclosed by a Marks decahedral cage of Au-rich sites. The surface is exclusively Ag–SR; X-ray absorption fine structure analysis supports the absence of Au–S bonds. The optical absorption spectrum shows a strong peak at 523 nm, seemingly a plasmon peak, but fs spectroscopic analysis indicates its non-plasmon nature. The non-metallicity of the $Au_{130-x}Ag_x$ nanocluster has set up a benchmark to study the transition to metallic state in the size evolution of bimetallic nanoclusters. The localized Au/Ag binary architecture in such a large alloy nanocluster provides atomic-level insights into the Au–Ag bonds in bimetallic nanoclusters.*

Alloying is a versatile strategy for tailoring the functionality of metal nanomaterials.[1] Alloy nanoparticles often exhibit enhanced performance compared to the monometallic counterparts.[2] For nanoalloys, the atomic distribution of metal elements (for example, in the core and/or surface) would significantly affect the functionality. Therefore, it is of great importance to precisely map out the heterometal positions. Recent advances in research on ultrasmall nanoparticles (so-called nanoclusters, NCs) have indeed demonstrated atomically resolved structural analysis of the heterometal sites in a NC by X-ray crystallography and also a precise quantification of such doping atoms by mass spectrometry.[3] These techniques allow new strategies to be explored to control the functionality by correlating the crystal structures and the observed properties.[3,4] The achievements in the ultrasmall size regime include the successful enhancement of intriguing properties unique to NCs, such as luminescence, catalysis, and electron dynamics.[5–7]

While much work has been done on the smaller sizes of NCs (less than 100 metal atoms), larger-size NCs (that is, >100 metal atoms) are still rare owing to major difficulties in the synthesis and crystallization.[8] For large bimetallic NCs, the reported structures are alkynyl-protected $Au_{80}Ag_{30}$[9] and $Au_{57}Ag_{53}$,[10] as well as thiolate-protected $Au_{267-x}Ag_x$.[11] Broadly speaking, it still remains a huge challenge to precisely control the synthesis and map out the dopant distribution in bimetallic nanostructures owing to the complexity.[12]

The major difficulties in large size NCs hamper the pursuit of clear answers to some fundamental questions of nanoscience, such as the dopant patterns and the effect on functionality, the transition from non-metallic to metallic state in alloy NCs. In homogold NCs, femtosecond spectroscopic analysis revealed a sharp transition from non-metallic to metallic state between Au_{246} and Au_{279}, which came together with structural analysis by X-ray crystallography.[13] Similar breakthroughs are expected for nanoalloys considering their outstanding functionality compared to monometallic nanomaterials. To understand the effects of size, structure, and Au/Ag ratios on the transition from quantized to metallic state, experimental approaches should include atomically precise structural analysis and the study on the properties, which has only been partially completed in previous studies.[11,14]

Here, we report the synthesis and structural determination of bimetallic $Au_{130-x}Ag_x(TBBT)_{55}$ NCs (average $x = 98$ and TBBT stands for S-Ph-*p*-$C(CH_3)_3$), together with spectroscopic analysis. X-ray crystallography reveals a drum-like pattern of Ag-rich sites enclosed in a Marks decahedral cage of Au-rich sites, and such a core is protected by a shell of Ag-SR (that is, no Au-SR). The observation of the localized binary architecture is interesting and provides insight into the dopant distribution in the Au/Ag alloy. X-ray absorption fine structure (XAFS) analysis confirms the absence of Au–S bonds. Femtosecond transient absorption (TA) spectroscopy reveals non-metallicity of $Au_{130-x}Ag_x(TBBT)_{55}$.

[*] T. Higaki, Prof. R. Jin
Department of Chemistry, Carnegie Mellon University
Pittsburgh, PA 15213 (USA)
E-mail: rongchao@andrew.cmu.edu
Dr. C. Liu, T.-Y. Luo, Prof. N. L. Rosi
Department of Chemistry, University of Pittsburgh
Pittsburgh, PA 15260 (USA)
D. J. Morris, Prof. P. Zhang
Department of Chemistry, Dalhousie University
Halifax, Nova Scotia B3H 4R2 (Canada)
Dr. G. He, Dr. M. Y. Sfeir
Center for Functional Nanomaterials
Brookhaven National Laboratory
Upton, NY 11973 (USA)
Dr. M. Y. Sfeir
Present address: Department of Physics, Graduate Center
City University of New York
New York, NY 10016 (USA)
and
Photonics Initiative, Advanced Science Research Center
City University of New York
New York, NY 10031 (USA)
Supporting information and the ORCID identification number(s) for the author(s) of this article can be found under: https://doi.org/10.1002/anie.201908694.

The $Au_{130-x}Ag_x$ alloy was synthesized by a size-focusing method and isolated by solvent fractionation (see Supporting Information for details). Briefly, $HAuCl_4{\cdot}3H_2O$ and $AgNO_3$ were mixed with HS-Ph-*p*-$C(CH_3)_3$, and slowly reduced by $NaBH_4$ in the presence of NaOH. The solution was stirred overnight for spontaneous size-focusing of the initially polydispersed NCs into a single-size product ($Au_{130-x}Ag_x$) with molecular purity. The product $Au_{130x}Ag_x$ was extracted by CH_2Cl_2 (DCM) after washing out impurities (for example, excess thiol) by methanol and toluene. Single-crystal growth of $Au_{130-x}Ag_x$ was done by gentle evaporation of solvent (DCM) from a concentrated DCM solution of the NCs.

The crystal structure of $Au_{130-x}Ag_x$ shows a bimetallic M_{54} (M = Au/Ag) core with a decahedral topology (Figure 1 A). In the bimetallic core, all the $Au_{\approx 32}$ atoms are localized in the truncated M_{49} Marks decahedron, whereas the five corners of the regular M_{54} decahedron comprise 100% Ag atoms (highlighted by arrows in Figure 1 B). This preferential

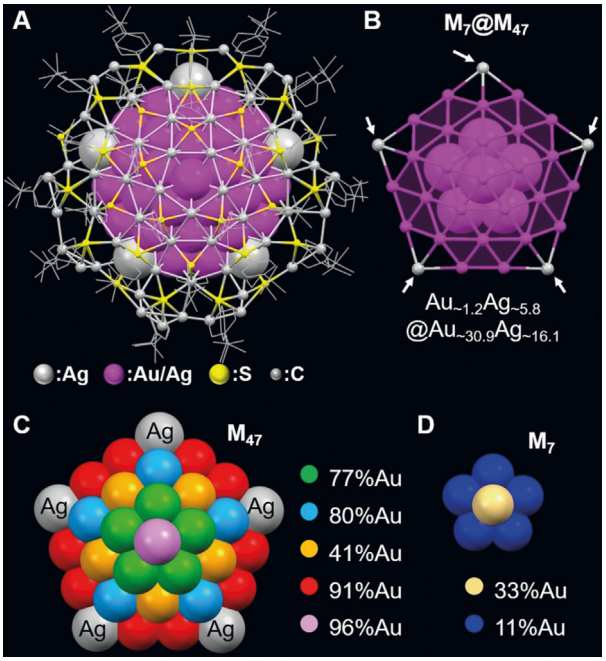

Figure 1. Crystal structure of the $Au_{130-x}Ag_x(TBBT)_{55}$ NCs: A) Total structure; B) Decahedral M_{54} core with shell-by-shell $M_7@M_{47}$ illustration (M = Au/Ag); C),D) Mapping of Au/Ag occupancy in the decahedral M_{54} core.

location of Au atoms is reminiscent of the Marks decahedral Au_{49} core in $Au_{102}(SR)_{44}$[15] and $Au_{103}S_2(SR')_{41}$.[16] The truncated decahedral cores (for example, Marks or Ino D_h) are often observed in large Au NCs[3a,17] as opposed to no truncation in Ag NCs. This is consistent with the higher surface energy of 1.55 $J\,m^{-2}$ for Au(111) than the 1.25 $J\,m^{-2}$ for Ag(111),[1] since truncation reduces the surface energy.[18] Thus, the interesting observation in the bimetallic $Au_{130-x}Ag_x$ structure may indicate that the structural rule of monometallic Au or Ag NCs can be applicable to alloy NCs of the two metals, which would be useful in future prediction of dopant distributions.[19]

Crystallographic analysis has also quantified the partial Au/Ag occupancy at each site of the decahedral M_{54} core, which comprises an inner M_7 and an outer M_{47} (Figure 1 C,D). The outer M_{47} comprises 42 Au-rich sites, with a total of about 31 Au atoms in composition (that is, $Au_{30.9}Ag_{16.1}$), but the remaining 5 sites (that is, the corners of the decahedron) are exclusively occupied by Ag (Figure 1 C). It is worth noting that the adjacent sites to these five Ag sites show actually very high Au occupancy (91% or 80%, shown in red and blue in Figure 1 C, error bar: ca. 1%), indicating the strong preference of Au atoms to avoid the corners and thus the formation of the truncated Marks-decahedron. In contrast, the inner M_7 core is made up of Ag-rich sites with minor Au occupancy (that is, 33% and 11%, Figure 1 D).

Further structural analysis is performed on the bond length distribution and comparison with the decahedral structures of Au_{102}/Au_{103} as well as Ag_{136} for comparable sizes.[8b,15,16] Overall, the bond length in $Au_{130-x}Ag_x$ showed a stepwise increase from the interior M_7 core to the outermost shell (Supporting Information, Figure S1). It is known that Au and Ag show similar diameters (1.44 Å for Au; 1.45 Å for Ag) and bond lengths, so alloying is considered to be less likely to deform the overall geometry.[1] However, some metal–metal bonds in the M_{54} core of $Au_{130-x}Ag_x$ have significantly different lengths compared to those in Au_{102}/Au_{103}, for example, five axial bonds (bond α in the Supporting Information, Figure S2) in the outer M_{47} of $Au_{130-x}Ag_x$ are 3.057 Å, being 7% longer than the neighboring axial bonds (bond β in the Supporting Information, Figure S2). In contrast, the same bonds in the same geometry in Au_{102}/Au_{103} are shorter (2.947 Å) and the difference with adjacent bonds is also smaller (5.7%). The specific bonds in Ag_{136} are also shorter (2.999 Å) and exhibit a smaller difference (6.0%) relative to the neighboring bonds in Ag_{136}.

To map out the overall Au/Ag distribution in $Au_{130-x}Ag_x$, Au-rich or Ag-rich sites are highlighted in Figure 2. At the innermost locations, the Ag-rich sites comprise a framework

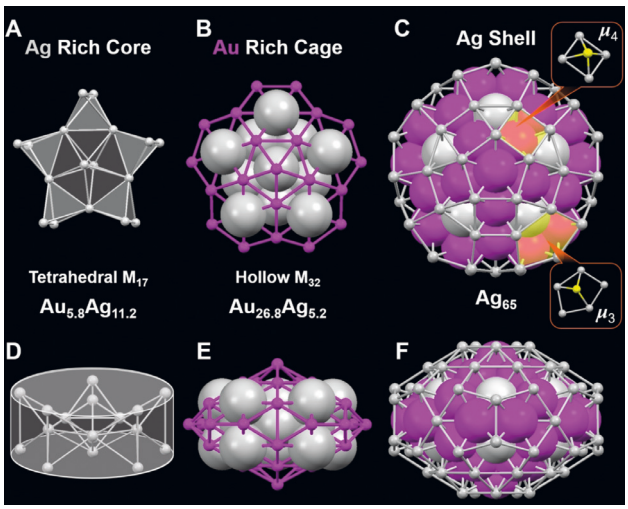

Figure 2. Anatomy of the structure of $Au_{130-x}Ag_x(TBBT)_{55}$: A) Ten tetrahedra in the Ag-rich M_{17} core; B) Au-rich M_{32} cage; C) Ag_{65} outermost shell protecting the M_{49} core; D)–F) side views of the binary M_{17}, M_{32}, and Ag_{65}.

by twinning ten M_4 tetrahedra (Figure 2A,D) resembling a drum. The drum of Ag-rich sites is then covered by an Au-rich cage of M_{32} ($Au_{26.8}Ag_{5.2}$), forming a truncated M_{49} Marks decahedron (Figure 2B,E). The M_{49} core is capped by an outermost shell of Ag_{65} with overall D_{5h} symmetry (Figure 2C,F). The top and bottom of the Ag_{65} cage are each exclusively protected by 15 bridging thiolates; among them, 5 bridging thiolates reside on the five Ag_4 squares (upper right inset in Figure 2C) to form a pentagonal arrangement in a μ_4 manner, another 5 thiolates on the adjacent Ag_4 squares, and the remaining 5 thiolates are bonded to the Ag_5 pentagons in a μ_3 manner (lower right inset in Figure 2C).

Further structural insights into the $Au_{130-x}Ag_x$ alloy was obtained by X-ray absorption spectroscopy. Au L_3-edge and Ag K-edge FT-EXAFS (Fourier transformed extended XAFS) of $Au_{130-x}Ag_x$ in the solid state are shown in the Supporting Information, Figure S3. Au L_3-edge FT-EXAFS showed a doublet peak in the range of 2–3 Å, indicating the alloy nature of Au/Ag in $Au_{130-x}Ag_x$, rather than intermetallic species with distinct Au/Ag locations and specific occupancy (Supporting Information, Figure S3A).[20] This observation is consistent with the partial Au/Ag occupancy by crystallography (Figure 1). Importantly, fitting analysis of Au L_3-edge FT-EXAFS reveals the absence of Au–S bonds in the $Au_{130-x}Ag_x$ NCs (Table 1). Thus, all Au atoms are localized inside the M_{49} core and the surface is exclusively made up of Ag–S motifs (Figure 2C), which is consistent with the conclusion by crystallographic analysis. In contrast, Ag K-edge FT-EXAFS clearly shows Ag–S bonds represented by the peak at about 2 Å, along with Ag–Ag and Ag–Au bonds (Table 1). The Au–Au and Au–Ag bond lengths are 2.84(5) and 2.84(1) Å, respectively, for $Au_{130-x}Ag_x$, which are comparable to other NCs with >100 metal atoms (for example, Au_{144}, $Au_{144-x}Ag_x$).[3b,14b,21]

Figure S4 shows Au L_3-edge and Ag K-edge XANES spectra of $Au_{130-x}Ag_x$. The relatively higher white-line intensity (main absorption peak) of $Au_{130-x}Ag_x$ in Au L_3-edge XANES indicates the loss of 5d electrons in Au atoms upon alloying with Ag, that is, d-electron transfer from Au to Ag, which is consistent with previous reports on bimetallic nanoparticles[22] and bulk of Au/Ag.[23] Note that this observation does not necessarily contradict the electronegativity rule as Au has been known to lose d electrons to Ag but gain non-d electrons in Au-Ag bulk alloys.[23] Overall, the XAFS analysis on the bimetallic NCs further supports the structural determination by crystallography and also reveals charge transfer inside the decahedral core.

The electronic structure of $Au_{130-x}Ag_x$ was analyzed by optical spectroscopy. The steady-state spectrum of $Au_{130-x}Ag_x$ shows a strong peak at 523 nm and a small hump at 764 nm (Figure 3). The absorption profile, especially the 523 nm peak, seems to be a plasmon resonance of Au/Ag alloy nanoparticles, but careful analysis ruled out this possibility (see below).

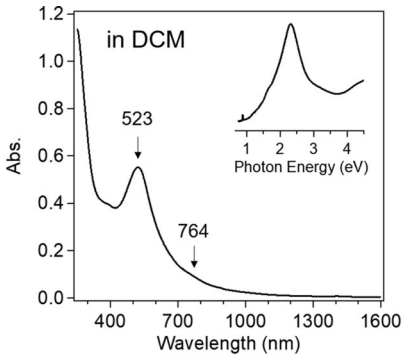

Figure 3. Steady-state optical absorption spectrum of $Au_{130-x}Ag_x$ NCs in DCM.

Table 1: Fitting results of Au L_3-edge and Ag K-edge FT-EXAFS spectra of $Au_{130-x}Ag_x$ bimetallic NCs.

Absorption edge	Bond	CN[a]	R [Å][b]	$\sigma^2\times10^{-3}$ [Å][c]	E_0 [eV][d,e]	R factor
Au L_3	Au–Au	3.8	2.84(5)	14(5)	4(1)	0.0237
	Au–Ag	5.3	2.84(1)[e]	9(1)	4(1)	
	Ag–S	1.3	2.449(8)	9(1)	−1.9(7)	
Ag K	Ag–Au	1.6	2.84(1)[e]	7(2)	−1.9(7)	0.0237
	Ag–Ag	2.1	2.84(1)	9(1)	−1.9(7)	

[a] Coordination number (CN). The values are from the crystal structure and fixed for fitting. [b] Bond length. [c] Debye–Waller factor. [d] Edge-energy shift. [e] Correlated for fitting.

To study the nature of the strong absorption band of $Au_{130-x}Ag_x$, femtosecond transient absorption (TA) spectroscopic analysis was performed (Figure 4). Upon photoexcitation at 480 nm, the TA spectra of $Au_{130-x}Ag_x$ showed a net ground state bleaching (GSB) band centered at about 530 nm and a small bleaching signal at about 760 nm (Figure 4A,B), which are consistent with the two peak positions in the steady-state spectrum (Figure 3). Broad excited state absorption (ESA) was also observed from 550 to 750 nm. The strong

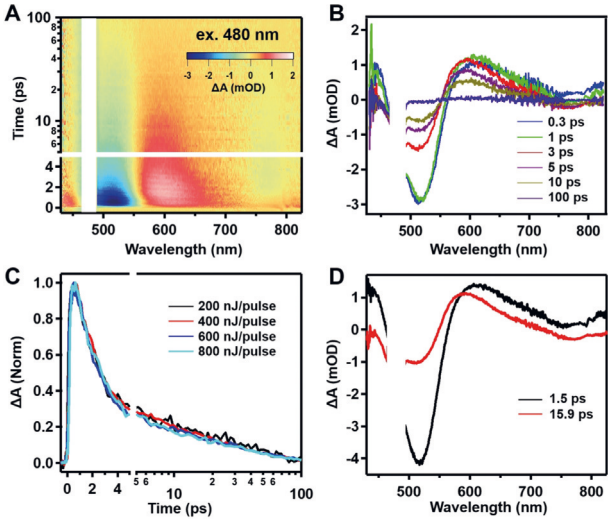

Figure 4. A) Transient absorption (TA) data map of $Au_{130-x}Ag_x$ pumped at 480 nm (in DCM); B) TA spectra as a function of time delay between 0.3 and 100 ps; C) normalized decay kinetics at 515 nm as a function of pump fluence; D) global fitting analysis of the TA data.

GSB at about 530 nm and broad ESA somewhat resemble the TA spectrum of plasmonic gold nanoparticles.[24] To probe whether the about 530 nm band is of plasmonic nature or not, we performed analysis on the decay kinetics as a function of pump fluence. Significantly, the decay process of $Au_{130-x}Ag_x$ showed no dependence on the pump pulse fluence, indicating its non-metallic state (Figure 4C).

Furthermore, global fitting analysis of the TA spectra revealed two decay processes with similar profiles (Figure 4D). The faster 1.5 ps process is assigned to internal conversion since the excitation (480 nm, 2.58 eV) is far above the band gap (< 1 eV, exact E_g not determined). The slower 15.9 ps process is assigned to the relaxation from the lowest excited-state to the ground state. Previous ultrafast spectroscopic studies revealed the long components of thiolate-protected NCs with about 100 metal atoms to be 420 ps for $Au_{103}S_2(SR)_{41}$,[16] 180 ps for $Au_{130}(SR)_{50}$,[25] 30 ps for $Au_{133}(SR)_{52}$,[26] and 325 ps for $Ag_{146}Br_2(SR)_{80}$,[27] which are all significantly longer than 15.9 ps observed in $Au_{130-x}Ag_x$. Considering the observed charge transfer in XAFS analysis, the shorter excited-state lifetime of $Au_{130-x}Ag_x$ could originate from its bimetallic nature. Further spectroscopic studies on bimetallic NCs are expected to reveal the origin of this faster relaxation than homometal NCs, such as the effect of structure, ligands, or Au/Ag ratios. Such efforts will be essential in exploring the transition from non-metallic to metallic state in alloy NCs.

In summary, the structural and spectroscopic analyses on the $Au_{130-x}Ag_x$ NCs have offered important insights into the Au/Ag alloying phenomenon. Specifically, a bimetallic M_{54} core exhibits five corners being exclusively of Ag (with no Au occupation), and all the Au atoms in the core are localized in the truncated M_{49} Marks decahedral sites. The formation of a golden Marks decahedron in alloy NCs is interesting and unprecedented. It provides useful rules for future structural prediction of large alloy NCs. Meticulous analysis on the whole structure has revealed that the $Au_{130-x}Ag_x$ consists of a drum-like architecture of Ag-rich sites enclosed in a Marks decahedral cage of Au-rich sites. XAFS analysis confirmed the absence of Au on the surface and also revealed charge transfer within the alloy structure. Steady-state and ultrafast spectroscopic analyses have revealed a non-metallic state of $Au_{130-x}Ag_x$, which provides a benchmark to map out the transition to non-metallic state for Au/Ag alloy NCs in future research. Overall, $Au_{130-x}Ag_x$ is the hitherto second largest Au/Ag alloy, and the obtained insights may open up new opportunities for tailoring the functionalities of alloys for catalysis, optics, and quantum-state control, as well as for bridging with plasmonic alloy nanoparticles.

Acknowledgements

R.J. acknowledges financial support from the National Science Foundation (DMR-1808675). This research also used resources of the Center for Functional Nanomaterials, which is a U.S. DOE Office of Science Facility, at Brookhaven National Laboratory under Contract No. DE-SC0012704. P.Z. thanks the NSERC Canada Discovery Grant for funding. CLS@APS facilities (Sector 20-BM) at the Advanced Photon Source (APS) are supported by the U.S. Department of Energy (DOE), NSERC Canada, the University of Washington, the Canadian Light Source (CLS), and the APS. Use of the APS is supported by the DOE under Contract no. DE-AC02-06CH11357. The CLS is financially supported by NSERC Canada, CIHR, NRC, and the University of Saskatchewan.

Conflict of interest

The authors declare no conflict of interest.

Keywords: alloys · crystal structure · electron dynamics · nanoclusters · X-ray spectroscopy

How to cite: *Angew. Chem. Int. Ed.* **2019**, *58*, 18798–18802
Angew. Chem. **2019**, *131*, 18974–18978

[1] a) R. Ferrando, J. Jellinek, R. L. Johnston, *Chem. Rev.* **2008**, *108*, 845–910; b) P.-C. Chen, M. Liu, J. S. Du, B. Meckes, S. Wang, H. Lin, V. P. Dravid, C. Wolverton, C. A. Mirkin, *Science* **2019**, *363*, 959–964; c) T. Yonezawa, N. Toshima, *New J. Chem.* **1998**, *22*, 1179–1201.

[2] a) L. Huang, P.-C. Chen, M. Liu, X. Fu, P. Gordiichuk, Y. Yu, C. Wolverton, Y. Kang, C. A. Mirkin, *Proc. Natl. Acad. Sci. USA* **2018**, *115*, 3764–3769; b) F. Chang, S. Shan, V. Petkov, Z. Skeete, A. Lu, J. Ravid, J. Wu, J. Luo, G. Yu, Y. Ren, C.-J. Zhong, *J. Am. Chem. Soc.* **2016**, *138*, 12166–12175; c) K. Mayer, J. Wessing, T. F. Fassler, R. A. Fischer, *Angew. Chem. Int. Ed.* **2018**, *57*, 14372–14393; *Angew. Chem.* **2018**, *130*, 14570–14593.

[3] a) R. Jin, C. Zeng, M. Zhou, Y. Chen, *Chem. Rev.* **2016**, *116*, 10346–10413; b) S. Yamazoe, T. Tsukuda, *Bull. Chem. Soc. Jpn.* **2019**, *92*, 193–204; c) I. Chakraborty, T. Pradeep, *Chem. Rev.* **2017**, *117*, 8208–8271; d) S. Wang, S. Jin, S. Yang, S. Chen, Y. Song, J. Zhang, M. Zhu, *Sci. Adv.* **2015**, *1*, e1500441; e) Y. Wang, X. K. Wan, L. Ren, H. Su, G. Li, S. Malola, S. Lin, Z. Tang, H. Häkkinen, B. K. Teo, Q.-M. Wang, N. Zheng, *J. Am. Chem. Soc.* **2016**, *138*, 3278–3281; f) Y. Li, T.-Y. Luo, M. Zhou, Y. Song, N. L. Rosi, R. Jin, *J. Am. Chem. Soc.* **2018**, *140*, 14235–14243; g) S. Hossain, Y. Niihori, L. V. Nair, B. Kumar, W. Kurashige, Y. Negishi, *Acc. Chem. Res.* **2018**, *51*, 3114–3124; h) K. Kwak, D. Lee, *Acc. Chem. Res.* **2019**, *52*, 12–22; i) T. Chen, Q. Yao, R. R. Nasaruddin, J. Xie, *Angew. Chem. Int. Ed.* **2019**, *58*, 11967–11977; *Angew. Chem.* **2019**, *131*, 12093–12103; j) M. S. Bootharaju, C. P. Joshi, M. R. Parida, O. F. Mohammed, O. M. Bakr, *Angew. Chem. Int. Ed.* **2016**, *55*, 922–926; *Angew. Chem.* **2016**, *128*, 934–938; k) S. Takano, H. Hirai, S. Muramatsu, T. Tsukuda, *J. Am. Chem. Soc.* **2018**, *140*, 12314–12317.

[4] a) T. Higaki, Y. Li, S. Zhao, Q. Li, S. Li, X. S. Du, S. Yang, J. Chai, R. Jin, *Angew. Chem. Int. Ed.* **2019**, *58*, 8291–8302; *Angew. Chem.* **2019**, *131*, 8377–8388; b) A. Ghosh, O. F. Mohammed, O. M. Bakr, *Acc. Chem. Res.* **2018**, *51*, 3094–3103; c) T. Higaki, C. Liu, C. Zeng, R. Jin, Y. Chen, N. L. Rosi, R. Jin, *Angew. Chem. Int. Ed.* **2016**, *55*, 6694–6697; *Angew. Chem.* **2016**, *128*, 6806–6809; d) C. Femoni, M. C. Iapalucci, S. Ruggieri, S. Zacchini, *Acc. Chem. Res.* **2018**, *51*, 2748–2755; e) Z. Gan, N. Xia, Z. Wu, *Acc. Chem. Res.* **2018**, *51*, 2774–2783; f) S. Wang, Q. Li, X. Kang, M. Zhu, *Acc. Chem. Res.* **2018**, *51*, 2784–2792.

[5] S. Wang, X. Meng, A. Das, T. Li, Y. Song, T. Cao, X. Zhu, M. Zhu, R. Jin, *Angew. Chem. Int. Ed.* **2014**, *53*, 2376–2380; *Angew. Chem.* **2014**, *126*, 2408–2412.

[6] a) S. Xie, H. Tsunoyama, W. Kurashige, Y. Negishi, T. Tsukuda, *ACS Catal.* **2012**, *2*, 1519–1523; b) H. Häkkinen, S. Abbet, A.

Sanchez, U. Heiz, U. Landman, *Angew. Chem. Int. Ed.* **2003**, *42*, 1297 – 1300; *Angew. Chem.* **2003**, *115*, 1335 – 1338; c) K. K. Chakrahari, R. P. B. Silalahi, T.-H. Chiu, X. Wang, N. Azrou, S. Kahlal, Y.-C. Liu, M.-H. Chiang, J.-Y. Saillard, C. W. Liu, *Angew. Chem. Int. Ed.* **2019**, *58*, 4943 – 4947; *Angew. Chem.* **2019**, *131*, 4997 – 5001.

[7] a) M. Zhou, T. Higaki, G. Hu, M. Y. Sfeir, Y. Chen, D. Jiang, R. Jin, *Science* **2019**, *364*, 279 – 282; b) K. Kwak, Q. Tang, M. Kim, D. E. Jiang, D. Lee, *J. Am. Chem. Soc.* **2015**, *137*, 10833 – 10840.

[8] a) C. Zeng, Y. Chen, K. Kirschbaum, K. J. Lambright, R. Jin, *Science* **2016**, *354*, 1580 – 1584; b) H. Yang, Y. Wang, X. Chen, X. Zhao, L. Gu, H. Huang, J. Yan, C. Xu, G. Li, J. Wu, A. J. Edwards, B. Dittrich, Z. Tang, D. Wang, L. Lehtovaara, H. Häkkinen, N. Zheng, *Nat. Commun.* **2016**, *7*, 12809; c) N. A. Sakthivel, S. Theivendran, V. Ganeshraj, A. G. Oliver, A. Dass, *J. Am. Chem. Soc.* **2017**, *139*, 15450 – 15459; d) Z. Lei, J. J. Li, X. K. Wan, W. H. Zhang, Q. M. Wang, *Angew. Chem. Int. Ed.* **2018**, *57*, 8639 – 8643; *Angew. Chem.* **2018**, *130*, 8775 – 8779; e) N. Yan, N. Xia, L. Liao, M. Zhu, F. Jin, R. Jin, Z. Wu, *Sci. Adv.* **2018**, *4*, eaat7259; f) S. Kenzler, C. Schrenk, A. Schnepf, *Angew. Chem. Int. Ed.* **2017**, *56*, 393 – 396; *Angew. Chem.* **2017**, *129*, 402 – 406; g) S. Vergara, D. A. Lukes, M. W. Martynowycz, U. Santiago, G. Plascencia-Villa, S. C. Weiss, M. J. De La Cruz, D. M. Black, M. M. Alvarez, X. López-Lozano, C. O. Barnes, G. Lin, H.-C. Weissker, R. L. Whetten, T. Gonen, M. J. Yacaman, G. Calero, *J. Phys. Chem. Lett.* **2017**, *8*, 5523 – 5530.

[9] J. L. Zeng, Z. J. Guan, Y. Du, Z. A. Nan, Y. M. Lin, Q.-M. Wang, *J. Am. Chem. Soc.* **2016**, *138*, 7848 – 7851.

[10] Z. Guan, J. Zeng, S. Yuan, F. Hu, Y. Lin, Q.-M. Wang, *Angew. Chem. Int. Ed.* **2018**, *57*, 5703 – 5707; *Angew. Chem.* **2018**, *130*, 5805 – 5809.

[11] J. Yan, S. Malola, C. Hu, J. Peng, B. Dittrich, B. K. Teo, H. Häkkinen, L. Zheng, N. Zheng, *Nat. Commun.* **2018**, *9*, 3357.

[12] S. J. L. Billinge, I. Levin, *Science* **2007**, *316*, 561 – 565.

[13] a) M. Zhou, C. Zeng, Y. Song, J. W. Padelford, G. Wang, M. Y. Sfeir, T. Higaki, R. Jin, *Angew. Chem. Int. Ed.* **2017**, *56*, 16257 – 16261; *Angew. Chem.* **2017**, *129*, 16475 – 16479; b) T. Higaki, M. Zhou, K. J. Lambright, K. Kirschbaum, M. Y. Sfeir, R. Jin, *J. Am. Chem. Soc.* **2018**, *140*, 5691 – 5695.

[14] a) H. Zheng, M. A. Tofanelli, C. J. Ackerson, K. L. Knappenberger, *Phys. Chem. Chem. Phys.* **2017**, *19*, 14471 – 14477; b) J. Liu, K. S. Krishna, C. Kumara, S. Chattopadhyay, T. Shibata, A. Dass, C. S. S. R. Kumar, *RSC Adv.* **2016**, *6*, 25368 – 25374.

[15] P. D. Jadzinsky, G. Calero, C. J. Ackerson, D. A. Bushnell, R. D. Kornberg, *Science* **2007**, *318*, 430 – 433.

[16] T. Higaki, C. Liu, M. Zhou, T. Y. Luo, N. L. Rosi, R. Jin, *J. Am. Chem. Soc.* **2017**, *139*, 9994 – 10001.

[17] Y. Chen, C. Zeng, C. Liu, K. Kirschbaum, C. Gayathri, R. R. Gil, N. L. Rosi, R. Jin, *J. Am. Chem. Soc.* **2015**, *137*, 10076 – 10079.

[18] a) L. D. Marks, L. Peng, *J. Phys. Condens. Matter* **2016**, *28*, 053001; b) A. I. Kirkland, P. P. Edwards, D. A. Jefferson, D. G. Duff, *Annu. Rep. Prog. Chem. Sect. C* **1990**, *87*, 247 – 304.

[19] A. Tlahuice-Flores, *Phys. Chem. Chem. Phys.* **2015**, *17*, 5551 – 5555.

[20] T. Shibata, B. A. Bunker, Z. Zhang, D. Meisel, C. F. Vardeman, J. D. Gezelter, *J. Am. Chem. Soc.* **2002**, *124*, 11989 – 11996.

[21] M. A. MacDonald, P. Zhang, H. Qian, R. Jin, *J. Phys. Chem. Lett.* **2010**, *1*, 1821 – 1825.

[22] S. Nishimura, A. T. N. Dao, D. Mott, K. Ebitani, S. Maenosono, *J. Phys. Chem. C* **2012**, *116*, 4511 – 4516.

[23] C. C. Tyson, A. Bzowski, P. Kristof, M. Kuhn, R. Sammynaiken, T. K. Sham, *Phys. Rev. B* **1992**, *45*, 8924 – 8928.

[24] a) G. V. Hartland, *Chem. Rev.* **2011**, *111*, 3858 – 3887; b) S. Link, M. A. El-Sayed, *Annu. Rev. Phys. Chem.* **2003**, *54*, 331 – 366.

[25] J. W. Padelford, M. Zhou, Y. Chen, R. Jin, G. Wang, *J. Phys. Chem. C* **2017**, *121*, 21217 – 21224.

[26] C. Zeng, Y. Chen, K. Kirschbaum, K. Appavoo, M. Y. Sfeir, R. Jin, *Sci. Adv.* **2015**, *1*, e1500045.

[27] Y. Song, K. Lambright, M. Zhou, K. Kirschbaum, J. Xiang, A. Xia, M. Zhu, R. Jin, *ACS Nano* **2018**, *12*, 9318 – 9325.

Manuscript received: July 12, 2019
Version of record online: November 8, 2019

